2024 European Control Conference (ECC)
June 25-28, 2024. Stockholm, Sweden

Energy-conserving discretization of the one-dimensional shallow water equations in material-fixed coordinates

Luca Mayer[1], Jens Wurm[2] and Frank Woittennek[3]

***Abstract*— A generalized approach to the spatial discretization of the one-dimensional shallow water equations with moving boundary and an arbitrary cross-section is developed. Material-fixed coordinates are used to effectively cope with the moving boundary. The methodology involves the discretization of the Lagrangian on a material-fixed grid and the application of different quadrature schemes to derive finite-dimensional models. The proposed scheme explicitly considers mass conservation as an additional constraint, resulting in systems of semi-explicit differential-algebraic equations (DAEs). The particular structure of these DAEs depends on the chosen quadrature scheme and therefore requires slightly different methods for the numerical implementation. These methods are discussed on the basis of three examples, which are compared in simulation studies.**

I. Introduction

The well-known Saint-Venant equations have long been instrumental in the modeling of shallow water flow in open channels. These equations find application in a multitude of scenarios, including the analysis of open-channel problems such as irrigation channels with varying cross-sections of riverbeds [3], [6], [4]. Furthermore, they have been extended to address unique challenges, such as the modeling of snow avalanches [13], [10]. In recent studies [7], [17], the focus has shifted towards control design for shallow water waves within tubes that feature a dynamic boundary and arbitrary cross-sections. These control strategies often require the use of observers to deduce the complete system state from selected point measurements. A crucial aspect of constructing these observers is the availability of accurate numerical models suitable for real-time implementation. These models depend on an appropriate discretization of the original spatially distributed model. To ensure that the stability properties of the initial model are preserved, energy-based methods are advantageous when deriving such approximations.

In [8], a family of approximated finite-dimensional models was introduced, aiming to retain the port-Hamiltonian structure of open systems models. This approach utilized conservative generalized leapfrog schemes with consistent orders and adopted a finite volume perspective on staggered grids.

The present contribution builds upon these foundations and focuses on the development of higher-order approximation schemes for a system akin to that considered in [18]. Specifically, we explore a boundary-actuated 1D shallow-water model with a moving boundary and an arbitrary cross-section. To address the challenges posed by the time-varying spatial domain in this model, we opt for a formulation using material-fixed coordinates, also known as Lagrange coordinates. Notably, the distributed shallow-water model can be derived using the principle of least action [15], [18], [11] , making both the action functional and the Lagrange functional key components in the derivation of our lumped approximation, i.e., the lumped parameter model. In particular, we discretize the Lagrange functional concerning space on a material-fixed grid and proceed to derive the finite-dimensional model by applying an appropriate quadrature scheme. Given the importance of mass conservation, this approach results in a system of semi-explicit differential-algebraic equations.

In contrast to [13], higher-order quadrature order quadrature schemes are introduced in [11]. Although this method is expected to provide more accurate numerical approximations, it leads to more complicated nonlinear DAEs. Therefore, different approaches to numerically solve the resulting DAEs are investigated in this paper.

The contribution is structured as follows: In section II, the model is introduced in both Eulerian and Lagrangian coordinates. Subsequently, spatially discrete models in the Lagrangian framework are then derived with a formulation compatible with arbitrary quadrature schemes. Section III examines the numerical solution of the resulting energy-conserving semi-discrete DAEs using three examples. Section IV provides a comparison of the derived models and their respective solution methods through simulations. Finally, section V contains a brief discussion and outlook on future research.

II. Modeling

A horizontally oriented tube is considered, as depicted in Figure 1, which is partially filled with a liquid. The tube has a total length L and a circular cross-sectional area with radius r. A moving piston is positioned at $z = l(t)$ opposite to the fixed wall at $z = 0$, altering the filled length $l(t)$ of the tube. The piston velocity $\dot{l}(t)$ serves as the input $u(t)$ to the system. One-dimensional shallow water models in Eulerian (spatially-fixed) and Lagrangian (material-fixed) coordinates

[1] Luca Mayer with Institute of Automation and Control Engineering, UMIT TIROL - Private University for Health Sciences and Health Technology, Eduard Wallnöfer Zentrum 1, Hall in Tirol, Austria luca.mayer@umit-tirol.at

[2] Jens Wurm with Institute of Automation and Control Engineering, UMIT TIROL - Private University for Health Sciences and Health Technology, Eduard Wallnöfer Zentrum 1, Hall in Tirol, Austria jens.wurm@umit-tirol.at

[3] Frank Woittennek with Institute of Automation and Control Engineering, UMIT TIROL - Private University for Health Sciences and Health Technology, Eduard Wallnöfer Zentrum 1, Hall in Tirol, Austria frank.woittennek@umit-tirol.at

are examined, with the Lagrangian formulation being derived using variational principles.

A. Eulerian coordinates

The dynamics of the system under consideration can be described by the one-dimensional Saint-Venant equations in spatially-fixed coordinates[1], also named Euler coordinates[16],

$$0 = A'(h)\left(\partial_t + v\partial_z\right)h + A(h)\partial_z v \tag{1a}$$
$$0 = g\partial_z h + \partial_t v + v\partial_z v, \tag{1b}$$

with the water level h and the mean horizontal velocity v of the fluid constituting the two distributed variables $(z,t) \mapsto (h,v) \in C_1(\Omega, \mathbb{R}^2)$ on the domain $\Omega = \{(z,t) | \, t \in \mathbb{R}^+, z \in [0, l(t)]\}$. Therein, $l(t)$ denotes the position of the piston, whose derivative serves as the input $u(t)$. Moreover, $A(h)$ with $A \in C_2\left([h_{\min}, h_{\max}], \mathbb{R}\right)$ strictly monotonically increasing is the portion of the cross-sectional area covered by the fluid, and g is the gravitational acceleration. The

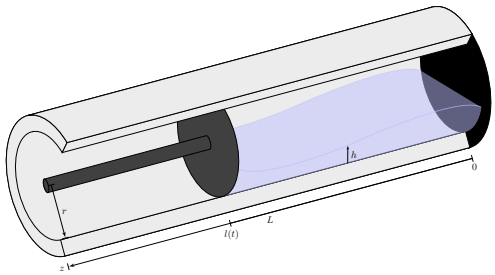

Fig. 1. Schematic of the considered setup.

boundary conditions (BCs)

$$v(0,t) = 0 \qquad \text{and} \qquad \int_0^{l(t)} A(h(z,t))\,\mathrm{d}z = V_{\mathrm{T}} \tag{1c}$$

of the partial differential equation (PDE) result from the fact that the velocity at the fixed boundary is zero and the total volume V_{T} of the fluid within the tube has to be constant[2]. Together with (1a) the second BC in (1c) implies (cf. [7] for details)

$$v(l(t),t) = \dot{l}(t) = u(t). \tag{1d}$$

For the case of a circular cross-section $A(h)$ is given by the area of a circular segment with the radius r:

$$A(h) = r^2 \arccos\left(1 - \frac{h}{r}\right) - (r-h)\sqrt{2rh - h^2},$$
$$A'(h) := \frac{\mathrm{d}A}{\mathrm{d}h}(h) = 2\sqrt{2rh - h^2}.$$

[1]See also [7] for a derivation of the model for the particular system under consideration.

[2]Discussion of well posedness of the above model is beyond the scope of the contribution. However, note that under additional assumptions, i.e., continuously differentiable initial data, corresponding to subcritical initial flow, and continuously differentiable input $t \mapsto \dot{l}(t)$, compatible with the initial conditions, local existence and uniqueness can be shown by integration along the characteristics (see, e.g., [2] for the underlying techniques).

For this representation, the kinetic energy $T(h(\cdot,t), v(\cdot,t))$ and the potential energy $U(h(\cdot,t))$ at time t are given by

$$T(h(\cdot,t), v(\cdot,t)) = \frac{\rho}{2}\int_0^{l(t)} A(h(z,t))v^2(z,t)\,\mathrm{d}z, \tag{2}$$
$$U(h(\cdot,t)) = \rho\, g \int_0^{l(t)} \int_0^{h(z,t)} \zeta A'(\zeta)\,\mathrm{d}\zeta\,\mathrm{d}z, \tag{3}$$

wherein ρ denotes the mass density of the medium.

B. Lagrangian coordinates

By introducing the independent variable $s \in \left[0, \bar{l}\right]$, the system variables

$$Z(s,t) = z \tag{4a}$$
$$\partial_t Z(s,t) = v(Z(s,t),t) =: V(s,t) \tag{4b}$$
$$H(s,t) = h(Z(s,t),t) \tag{4c}$$

are transformed into a material-fixed frame [1] constituting the two distributed variables $(s,t) \mapsto (H,V) \in C_1\left[\Omega_\ell, \mathbb{R}^2\right]$ on the domain $\Omega_\ell = \left\{(s,t) | \, t \in \mathbb{R}^+, s \in \left[0, \bar{l}\right]\right\}$. Therein, s corresponds to a particular fluid element located at $z = s$ in a given reference equilibrium associated with a particular piston position $\bar{l}$. Applying (4) to the mass conservation equation (1a)

$$\begin{aligned} 0 &= A'(H(s,t))\partial_t H(s,t) + \frac{A(H(s,t))}{\partial_s Z(s,t)}\partial_s\partial_t Z(s,t) \\ &= \partial_t\left(A(H(s,t))\partial_s Z(s,t)\right) \end{aligned}$$

and taking into account the reference configuration leads to the mass conservation equation in material-fixed coordinates

$$A(H(s,t))\partial_s Z(s,t) = A_0, \qquad A_0 = \frac{V_{\mathrm{T}}}{\bar{l}}. \tag{5a}$$

Moreover, applying the transformation (4) to the momentum balance (1b) yields

$$0 = \partial_t V(s,t) - \frac{g}{A_0}A(H(s,t))\partial_s H(s,t). \tag{5b}$$

The boundary conditions in (1c) translate into

$$Z(0,t) = 0, \qquad Z(\bar{l},t) = l(t), \tag{5c}$$

while the control input is given by $\partial_t Z(\bar{l},t) = \dot{l}(t) =: u(t)$.

Finally, the kinetic energie $T(V(\cdot,t))$ and the potential energie $U(H(\cdot,t))$, which have been introduced in (3), can be rewritten as

$$T(V(\cdot,t)) = \frac{\rho}{2}\int_0^{\bar{l}} A_0 V(s,t)^2\,\mathrm{d}s, \tag{6a}$$
$$U(H(\cdot,t)) = A_0\rho\, g \int_0^{\bar{l}} u(H(s,t))\,\mathrm{d}s, \tag{6b}$$
$$u(h) = \frac{1}{A(h)}\int_0^h \zeta\,\mathrm{d}A(\zeta). \tag{6c}$$

C. Energy conserving discretization

Within this section, energy-conserving approximations of the model equations are derived, employing the principle of least action. The main motivation for these discretization schemes is the following result borrowed from [18], [11] and being mainly a restatement of the earlier result [15] in material fixed coordinates. The equations of motion (5) result from the first-order stationary conditions deduced from

$$\delta \int_0^\tau \bar{\mathcal{L}}(H(\cdot,t), Z(\cdot,t), \partial_t Z(\cdot,t), \lambda(\cdot,t))\,\mathrm{d}t = 0$$

where the integrand

$$\bar{\mathcal{L}}(H, Z, \partial_t Z, \lambda) = T(V) - U(H) + C(H, Z, \lambda) \tag{7}$$

corresponds to the Lagrangian

$$\mathcal{L}(H, V) = T(V) - U(H)$$

augmented by the constraint term

$$\begin{aligned} &C(H(\cdot,t), Z(\cdot,t), \lambda(\cdot,t)) = \\ &\rho A_0 \int_0^{\bar{l}} \lambda(s,t)\,(A_0 - A(H(s,t))\partial_s Z(s,t))\;\mathrm{d}s \end{aligned} \tag{8}$$

obtained by adjoining the conservation of mass (5a) via the Lagrange multiplier $\lambda(s,t)$. To obtain the desired spatially discrete models, the Lagrangian (7) is approximated using different quadrature schemes. In order to facilitate this approximation, the spatial domain is divided into N intervals of equal length Δs

$$s_i = i\Delta s, \qquad s_N = \bar{l}, \qquad \Delta s = \frac{\bar{l}}{N}, \qquad i = 0, \ldots, N$$

with the system variables in $\boldsymbol{z} = (z_0, \ldots, z_N)^\intercal$, $\boldsymbol{h} = (h_0, \ldots, h_N)^\intercal$, defined by

$$\begin{aligned} z_i(t) &= Z(s_i, t), \\ v_i(t) &= \dot{z}_i(t) = \partial_t Z(s_i, t), \\ h_i(t) &= H(s_i, t). \end{aligned}$$

Subsequently, different quadrature formulae are applied in order to discretize the Langrange functional and the constraints on the above introduced grid. Applying the principle of least action to the resulting functional delivers the desired finite-dimensional model equations as a system of semi-explicit DAEs. Independently of the particular quadrature scheme applied, the kinetic energy and the potential energy are approximated in the form

$$\begin{aligned} T(\partial_t Z) \approx \hat{T}(\dot{\boldsymbol{z}}) &= \frac{1}{2}\dot{\boldsymbol{z}}^\intercal \boldsymbol{M}\dot{\boldsymbol{z}}, \\ U(H) \approx \hat{U}(\boldsymbol{h}) &= \boldsymbol{r}^\intercal \boldsymbol{u}(\boldsymbol{h}), \\ \boldsymbol{u}(\boldsymbol{h}) &= g\rho\bar{V}_\mathrm{T}\big(u(h_0), \ldots, u(h_N)\big)^\intercal, \end{aligned}$$

with the normalized potential energy density $u(h)$ defined in (6) and the constant volume within one spatial element $\bar{V}_\mathrm{T} = A_0\Delta s$. The positive vector $\boldsymbol{r} \in \mathbb{R}^{N+1}$ and the diagonal matrix $\boldsymbol{M} = \rho\bar{V}_\mathrm{T}\mathrm{diag}(\boldsymbol{r})$ depend on the particular scheme considered. Moreover, the constraints resulting from the conservation of mass are replaced by a finite number N_c of constraints of the form

$$\begin{aligned} \boldsymbol{0} &= \boldsymbol{G}\boldsymbol{z} - \boldsymbol{H}\boldsymbol{c}(\boldsymbol{h}), \\ \boldsymbol{c}(\boldsymbol{h}) &= \left(\frac{\bar{V}_\mathrm{T}}{A(h_0)}, \ldots, \frac{\bar{V}_\mathrm{T}}{A(h_N)}\right)^\intercal \end{aligned} \tag{9}$$

with $\boldsymbol{G}, \boldsymbol{H} \in \mathbb{R}^{N_c \times (N+1)}$ depending on the integration scheme considered. The latter are obtained by rewriting (5a) in integral form

$$\int_{s_i}^{s_j} \frac{A_0}{A(H(s,t))}\,\mathrm{d}s = Z(s_j, t) - Z(s_i, t), \quad i, j \in \{0, \ldots, N\}$$

for particular pairs (i, j) and applying the quadrature scheme of interest. Adjoining these constraints to the discrete Lagrange function $\hat{\mathcal{L}}(\boldsymbol{h}, \dot{\boldsymbol{z}}) = \hat{T}(\dot{\boldsymbol{z}}) - \hat{U}(\boldsymbol{h})$ via the Lagrange multipliers in $\boldsymbol{\lambda} \in \mathbb{R}^{N_c}$ and, additionally, taking into account the kinematic constraints $z_0 = 0$, $l = z_N$ via the multipliers $\bar{\lambda}_0$ and $\bar{\lambda}_N$, the variational problem to be considered for the derivation of the finite-dimensional model is given by

$$\begin{aligned} \delta \int_0^\tau \Big(&\hat{\mathcal{L}}(\boldsymbol{h}(t), \dot{\boldsymbol{z}}(t)) + \boldsymbol{\lambda}^\intercal(t)\,(\boldsymbol{G}\boldsymbol{z}(t) - \boldsymbol{H}\boldsymbol{c}(\boldsymbol{h}(t))) \\ &+ \bar{\lambda}_0(t) z_0(t) + \bar{\lambda}_N(t)(z_N(t) - l(t)) \Big)\,\mathrm{d}t = 0. \end{aligned}$$

Evaluating the variational derivatives and integrating by parts, after some intermediate calculations, yields the finite-dimensional formulation of the equations of motion:

$$\boldsymbol{M}\ddot{\boldsymbol{z}} = \boldsymbol{G}^\intercal\boldsymbol{\lambda} + \boldsymbol{e}_0\bar{\lambda}_0 + \boldsymbol{e}_N\bar{\lambda}_N \tag{10a}$$

$$\boldsymbol{H}^\intercal\boldsymbol{\lambda} = -\boldsymbol{R}\,\boldsymbol{I}(\boldsymbol{h}), \tag{10b}$$

$$\boldsymbol{I}(\boldsymbol{h}) = g\rho\left(\int_0^{h_0} A(\zeta)\,\mathrm{d}\zeta, \ldots, \int_0^{h_N} A(\zeta)\,\mathrm{d}\zeta\right)^\intercal$$

with $\boldsymbol{R} = \mathrm{diag}(\boldsymbol{r})$, $\boldsymbol{e}_i = (\kappa_{0i}, \ldots, \kappa_{iN})$ and κ_{ij} being the Kronecker delta. The model is completed by the kinematic constraints $z_0 = 0$, $z_N = l$ and the mass-conservation (9). Note that the Hamiltonian

$$\hat{\mathcal{H}}(\boldsymbol{h}, \dot{\boldsymbol{z}}) = \frac{\partial\hat{\mathcal{L}}}{\partial\dot{\boldsymbol{z}}}(\boldsymbol{h}, \dot{\boldsymbol{z}})\dot{\boldsymbol{z}} - \hat{\mathcal{L}}(\boldsymbol{h}, \dot{\boldsymbol{z}}) = \hat{T}(\dot{\boldsymbol{z}}) + \hat{U}(\boldsymbol{h}),$$

associated with the above-defined variational problem, satisfies

$$\frac{\mathrm{d}}{\mathrm{d}t}\hat{\mathcal{H}}(\boldsymbol{h}(t), \dot{\boldsymbol{z}}(t)) = -\bar{\lambda}_N\dot{l}(t).$$

In particular, for a constant position of the piston, energy conservation is retained in the approximation.

III. Numerical solution

The numerical solution strategy of the resulting DAEs depends not only on the chosen approximation method, but also on the number of constraints. Based on the equations of motion (10) including the associated constraints (9), several solution paths are examined in this section using three different quadratures as examples, namely the trapezoidal rule, Simpson's rule and Simpson's $3/8$ rule. Independent of quadrature and numerical solution, the reference conditions are as follows: The system is in a steady state, i.e. a constant height profile, zero fluid velocity, hence a spatial discretization with equal step size.

A. Trapezoidal rule

First, the trapezoidal approximation of the Lagrangian (7) is examined. This procedure is illustrated in Fig. 2, where the green lines show the approximation within the schematic representation of the spatial domain for each spatial element. By applying this quadrature to the spatial discretization

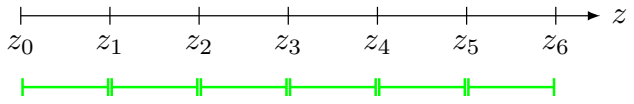

Fig. 2. Approximation of the Lagrangian using the trapezoidal rule with $N = 6$ volume elements.

scheme from the Section II-C, the matrices occuring in the model equations (9) and (10) read ($N_c = N$):

$$\boldsymbol{r}^\intercal = \frac{1}{2}(1, 2, \ldots, 2, 1), \tag{11a}$$

$$\boldsymbol{G} = (G_{ij})_{i=1,\ldots,N,j=0,\ldots,N}, \tag{11b}$$

$$\boldsymbol{H} = (H_{ij})_{i=1,\ldots,N,j=0,\ldots,N}, \tag{11c}$$

where the entries of $\boldsymbol{G}$ and $\boldsymbol{H}$ are given by:

$$G_{ij} = -\kappa_{(i-1)j} + \kappa_{ij},$$
$$H_{ij} = \frac{1}{2}(\kappa_{(i-1)j} + \kappa_{ij}).$$

With this in mind, the equations of motion and the constraints now take the form

$$\boldsymbol{f}(\boldsymbol{\lambda}) = \boldsymbol{M}^{-1}\boldsymbol{G}^\intercal\boldsymbol{\lambda} = \dot{\boldsymbol{v}}, \tag{12a}$$

$$\boldsymbol{g}(\boldsymbol{h}, \boldsymbol{z}, \boldsymbol{\lambda}) = \boldsymbol{G}\boldsymbol{z} - \boldsymbol{H}\boldsymbol{\varphi} = \boldsymbol{0}, \tag{12b}$$

using the composition

$$\boldsymbol{\varphi} = \boldsymbol{c} \circ \boldsymbol{I}^{-1}(-\boldsymbol{R}^{-1}\boldsymbol{H}^\intercal\boldsymbol{\lambda}) \tag{12c}$$

formed by (9) and (10b). The inverse function $\boldsymbol{I}^{-1}$ is evaluated numerically in advance for sufficiently many values for $\boldsymbol{I}(\boldsymbol{h})$ from the interval $[0, 2r]$ and interpolated during the simulation. The necessity of this composition is given by the number of constraints N_c and the dimensions of $\boldsymbol{G}$ or $\boldsymbol{H}$. In order to solve (12), index reduction with the use of differentiation is applied (see e.g. [14]). Therefore, (12b) can be rewritten as

$$\dot{\boldsymbol{g}}(\boldsymbol{h}, \boldsymbol{z}, \boldsymbol{\lambda}) + \boldsymbol{S}\boldsymbol{g}(\boldsymbol{h}, \boldsymbol{z}, \boldsymbol{\lambda}) = 0 \tag{13}$$

with its derivative

$$\dot{\boldsymbol{g}}(\boldsymbol{h}, \boldsymbol{z}, \boldsymbol{\lambda}) = \boldsymbol{G}\dot{\boldsymbol{z}} + \boldsymbol{H}\boldsymbol{C}_h\left(\boldsymbol{R}\boldsymbol{I}_h\right)^{-1}\boldsymbol{H}^\intercal\dot{\boldsymbol{\lambda}}, \tag{14}$$

the partial derivatives of the composition (12c) as diagonal matrices

$$\boldsymbol{C}_h = \operatorname{diag}\left(-\bar{V}_\mathrm{T}\frac{A'(\boldsymbol{h})}{A(\boldsymbol{h})^2}\right),$$
$$\boldsymbol{I}_h = \operatorname{diag}\left(\rho g A(\boldsymbol{h})\right),$$

and the Hurwitz matrix $\boldsymbol{S} \in \mathbb{R}^{N\times N}$ so that the solution of (13) converges against (12b). By substituting (14) in (13), the dynamics of the Lagrange multiplicators are given by

$$\dot{\boldsymbol{\lambda}} = -\left(\boldsymbol{H}\boldsymbol{C}_h\left(\boldsymbol{R}\boldsymbol{I}_h\right)^{-1}\boldsymbol{H}^\intercal\right)^{-1}\left(\boldsymbol{G}\dot{\boldsymbol{z}} + \boldsymbol{S}(\boldsymbol{G}\boldsymbol{z} - \boldsymbol{H}\boldsymbol{\varphi})\right).$$

Consequently, $\boldsymbol{\lambda}$ is part of the system state and is used to integrate (12a).

B. Modified composite Simpson's rule

The next approach is a modified composite Simpson's rule approximation of the Lagrangian (7). Similar to the trapezoidal rule, the red lines show the Simpson's rule approximation in Fig. 3. Therein, for even N, the spatial domain is approximated using the composite Simpson's rule applied to $N/2$ consecutive intervals of length $2\Delta s$. Secondly, the same procedure is used to approximate the integral over the interval $[\Delta s, (N-1)\Delta s]$, while the integrals over the boundary intervals $[0, \Delta s]$ and $[(N-1)\Delta s, N\Delta s]$ are approximated using the trapezoidal rule, displayed in green color. This approximation also works for an odd number of elements N, where the first iteration is performed up to the $N-1$ element and the second iteration is shifted accordingly. Finally, the approximation is calculated as the arithmetic mean of both approximations [11]. Using the described and

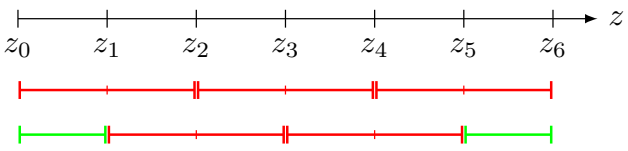

Fig. 3. Approximation of the Lagrangian using Simpson's rule with $N = 6$ volume elements.

in Fig. 3 illustrated approximation, the matrices occuring in the model euqations read ($N_c = N + 1$):

$$\boldsymbol{r}^\intercal = \frac{1}{12}(5, 13, 12, \ldots, 12, 13, 5), \tag{15a}$$

$$\boldsymbol{G} = (G_{ij})_{i,j=0,\ldots,N}, \tag{15b}$$

$$\boldsymbol{H} = (H_{ij})_{i,j=0,\ldots,N}, \tag{15c}$$

where the entries of $\boldsymbol{G}$ and $\boldsymbol{H}$ are given by $i = 1, \ldots, N-1$, $j = 0, \ldots, N$:

$$G_{0j} = \kappa_{1j} - \kappa_{0j},$$
$$G_{ij} = \kappa_{(i+1)j} - \kappa_{(i-1)j},$$
$$G_{Nj} = \kappa_{Nj} - \kappa_{(N-1)j},$$
$$H_{0j} = \tfrac{1}{2}(\kappa_{0j} + \kappa_{1j}),$$
$$H_{ij} = \tfrac{1}{3}(\kappa_{(i-1)j} + 4\kappa_{ij} + \kappa_{(i+1)j}),$$
$$H_{Nj} = \tfrac{1}{2}(\kappa_{(N-1)j} + \kappa_{Nj}).$$

The equations of motion and the constraints can be written as

$$\boldsymbol{f}(\boldsymbol{\lambda}) = \boldsymbol{M}^{-1}\boldsymbol{G}^\intercal\boldsymbol{\lambda} = \dot{\boldsymbol{v}}, \tag{16a}$$

$$\boldsymbol{g}(\boldsymbol{h}, \boldsymbol{z}, \boldsymbol{\lambda}) = \boldsymbol{H}^\intercal\boldsymbol{\lambda} + \boldsymbol{R}\boldsymbol{\varphi} = \boldsymbol{0}, \tag{16b}$$

with the composition

$$\boldsymbol{\varphi} = \boldsymbol{I} \circ \boldsymbol{c}^{-1}(\boldsymbol{H}^{-1}\boldsymbol{G}\boldsymbol{z}) \tag{16c}$$

formed by (9) and (10b). Given that $\boldsymbol{G}, \boldsymbol{H}$ are invertible and therefore regular matrices, solving (16) is straightforward. The only nonlinearity to be evaluated within this procedure

is the inverse function $\boldsymbol{c}^{-1}$ which is evaluated numerically in advance for sufficiently many values from the interval $[0, 2r\pi]$ and interpolated during the simulation.

C. Modified composite Simpson's 3/8 rule

The last example uses a modified composite Simpson's 3/8 rule to approximate the Lagrangian (7). In Fig. 4, this approximation with different quadratures is shown schematically. The blue lines indicate the approximation with Simpson's 3/8 rule. The green and red lines represent, as before, the trapezoidal and Simpson's rule, respectively. In the first

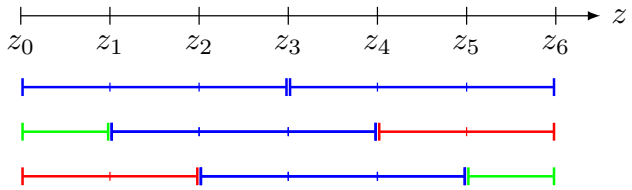

Fig. 4. Approximation of the Lagrangian using Simpson's 3/8 rule with $N = 6$ volume elements.

step, the spatial domain is approximated using the composite Simpson 3/8 rule for consecutive intervals of length $3\Delta s$. In the next two iterations the successive intervals are shifted accordingly. The remaining boundary elements are approximated according to their consecutive length using the trapezoidal rule for Δs or Simpson's rule for $2\Delta s$ (cf. Fig. 4). Finally, the approximation is calculated as the arithmetic mean of all three approximations. Within this example, the matrices occuring in the model euqations read ($N_c = N+2$):

$$\boldsymbol{r}^\intercal = \frac{1}{72}(29, 80, 71, 72, \ldots, 72, 71, 90, 29), \tag{17a}$$
$$\boldsymbol{G} = (G_{ij})_{i=0,\ldots,N+1,\, j=0,\ldots,N}, \tag{17b}$$
$$\boldsymbol{H} = (H_{ij})_{i=0,\ldots,N+1,\, j=0,\ldots,N}, \tag{17c}$$

where the entries of $\boldsymbol{G}$ and $\boldsymbol{H}$ are given by $i = 2, \ldots, N-1$, $j = 0, \ldots, N$:

$$\begin{aligned}
G_{0j} &= \kappa_{1j} - \kappa_{0j},\\
G_{1j} &= \kappa_{2j} - \kappa_{0j},\\
G_{ij} &= \kappa_{(i+1)j} - \kappa_{(i-2)j},\\
G_{Nj} &= \kappa_{Nj} - \kappa_{(N-2)j},\\
G_{(N+1)j} &= \kappa_{Nj} - \kappa_{(N-1)j},\\
H_{0j} &= \tfrac{1}{2}(\kappa_{0j} + \kappa_{1j}),\\
H_{1j} &= \tfrac{1}{3}(\kappa_{0j} + 4\kappa_{1j} + \kappa_{2j}),\\
H_{ij} &= \tfrac{3}{8}(\kappa_{(i-2)j} + 3\kappa_{(i-1)j} + 3\kappa_{ij} + \kappa_{(i+1)j}),\\
H_{Nj} &= \tfrac{1}{3}(\kappa_{(N-2)j} + 4\kappa_{(N-1)j} + \kappa_{Nj}),\\
H_{(N+1)j} &= \tfrac{1}{2}(\kappa_{(N-1)j} + \kappa_{Nj}).
\end{aligned}$$

Preliminary mathematical preparations are required before the resulting DAEs take a form akin to the previous examples. This need arises from the dimensions of $\boldsymbol{G}$ and $\boldsymbol{H}$, resulting from the number of constraints $N_c = N + 2$ (cf. Fig. 4). Let $\boldsymbol{v}^\intercal$ be an annihilator such that $\boldsymbol{v}^\intercal \boldsymbol{H} = \boldsymbol{0}$, the constraints (9) and its derivative read

$$\begin{aligned}
\boldsymbol{v}^\intercal \boldsymbol{G}\boldsymbol{z} &= \boldsymbol{v}^\intercal \boldsymbol{H}\boldsymbol{c}(\boldsymbol{h}) = \boldsymbol{0},\\
\boldsymbol{v}^\intercal \boldsymbol{G}\ddot{\boldsymbol{z}} &= \boldsymbol{0}.
\end{aligned} \tag{18}$$

Subsequently, by substituting (18) in (10a)

$$\boldsymbol{v}^\intercal \boldsymbol{G}\boldsymbol{M}\ddot{\boldsymbol{z}} = \boldsymbol{v}^\intercal \boldsymbol{G}\boldsymbol{G}^\intercal \boldsymbol{\lambda} = \boldsymbol{0}, \tag{19}$$

the equations of motion and the constraints can be stated as

$$\boldsymbol{f}(\boldsymbol{\lambda}) = \boldsymbol{M}^{-1}\boldsymbol{G}^\intercal \boldsymbol{\lambda} = \dot{\boldsymbol{v}}, \tag{20a}$$
$$\boldsymbol{g}(\boldsymbol{h}, \boldsymbol{z}, \boldsymbol{\lambda}) = \begin{bmatrix} \boldsymbol{H}^\intercal \\ \boldsymbol{v}^\intercal \boldsymbol{G}\boldsymbol{G}^\intercal \end{bmatrix} \boldsymbol{\lambda} + \begin{bmatrix} \boldsymbol{R}\,\boldsymbol{I}(\boldsymbol{h}) \\ 0 \end{bmatrix} = \boldsymbol{0}, \tag{20b}$$

where the constraint is formed by (19) and (10b).

IV. Simulation Study

In this section, the three discrete models of trapezoidal (12), modified composite Simpson's (16) and modified composite Simpson's 3/8 (17) rule are compared by simulation. Therein, the model in material-fixed coordinates approximated using the finite-difference method (FDM) w.r.t. space is used as benchmark. Moreover, an additional damping term as described in [18] was considered for all models (cf. Tab. I). Therefore, the variation of the Lagrangian is extended by the virtual work

$$\delta\mathcal{W}(Z, \partial_t Z) = \int_0^{\bar{l}} \mathcal{F}\left(\partial_t Z(s,t)\right) \delta Z(s,t)\, \mathrm{d}s$$

due to the friction with a force density $\mathcal{F}(\partial_t Z(\cdot,t))$ given by

$$\mathcal{F}(\partial_t Z(\cdot,t)) = D_\mathrm{f}\partial_s^2\left(\partial_t Z(\cdot,t)\right) = D_\mathrm{f}\partial_s^2 V(\cdot,t).$$

This results in an approximation

$$\mathcal{F}_i(\dot{z}_i(t)) = D_\mathrm{f}\left(\frac{\dot{z}_{i+1}(t) - 2\dot{z}_i(t) + \dot{z}_{i-1}(t)}{\Delta s}\right) \tag{21}$$

to be considered in the right-hand side of (10). Fig. 6 shows the four described models for a polynomial transition of the piston. Therein, the fluid height $h(0,t)$ at the fixed boundary and $h(l(t),t)$ at the moving boundary, the energy $\mathcal{H}(t)$ as well as the position $l(t)$ and the velocity $\dot{l}(t)$ of the piston are shown. As expected, the comparison of the wave propagation velocities and the height profiles at both system boundaries between the the models leads to similar results. However, with increasing polynomial degree in the quadrature scheme, higher oscillating modes occur, and the damping term needs to be chosen accordingly to maintain accuracy in integration. Furthermore, it can be observed that the total energy of the considered models decreases with time only due to the implemented damping, whereas the total energy of the FDM method additionally experiences a numerical damping, similar to fully discrete methods e.g. the Preissmann scheme [7].

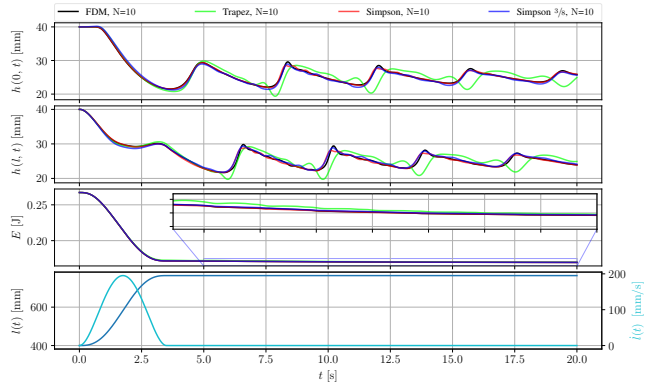

Fig. 5. Simulation results for a planned polynomial transition of the piston from $z_N(0\text{s}) = 400\text{mm}$ to $z_N(3{,}5\text{s}) = 764\text{mm}$ in 3,5s, which corresponds to a change of the fluid level starting from an initial height $\boldsymbol{h}(0) = 40\text{mm}$ to $\boldsymbol{h}(3{,}5\text{s}) = 25\text{mm}$. The number of spatial discretization points is $N = 10$ for all models.

	FDM	Trapezoidal	Simpson	Simpson 3/8
D_f	0,01	0,03	0,05	0,05

TABLE I

DAMPING TERMS USED IN SIMULATION

Python 3.10.12 and the latest NumPy[3] libraries were used to run the simulations. As the implementation of the proposed schemes is still to be optimized and the total runtime of the simulation strongly depends on the parameters chosen for the underlying adaptive Runge-Kutta schemes, total computation times presented below are of limited value. However, they show that, although required time for the energy-based methods is significantly higher than for a simple finite-difference scheme (cf. Tab. II), at least the modified composite Simpson's rule allows for real-time simulation with the chosen resolution. This efficiency is attributed to

	FDM	Trapezoidal	Simpson	Simpson 3/8
$N = 6$	0,26s	4,47s	5,41s	6,76s
$N = 10$	0,54s	27,31s	8,54s	95,07s

TABLE II

COMPUTATION TIME WITH INCREASING RESOLUTION[4]

the rather simple structure of the the resulting semi-explicit DAE. In contrast, the other two approximation schemes require more sophisticated computational schemes, including techniques like index reduction by differentiation.

V. CONCLUSION AND OUTLOOK

Energy-conserving semi-discrete approximations of the shallow-water equations with moving boundary have been derived. Since the solution of these approximations depends on the chosen approximation method or the number of constraints, three different numerical solution paths have been discussed and compared by low-resolution simulations. In addition to higher resolution simulations, these models will be compared with alternative numerical methods such as the Godunov scheme [5], pseudo-spectral approximations [12], or the method of characteristics. In the same way, besides spatial discretization, time integration using variational integrators [9] will be part of future research. Moreover, an open-loop control based on the shallow water equations in material-fixed coordinates will be derived and simulated using the methodology and numerical solutions presented in this paper.

[3]NumPy 1.26.4

[4]Specifications of the PC used for simulation:

- CPU: Intel® Core™ i5 − 10210U @ 1,60GHz × 8
- RAM: 16,0G

REFERENCES

[1] J. M. Augenbaum. A Lagrangian method for the shallow water equations based on a Voronoi mesh-one dimensional results. *Journal of Computational Physics*, 53(2):240–265, 1984.

[2] A. Bressan. *Hyperbolic Systems of Conservation Laws: The One-dimensional Cauchy Problem*. Oxford University Press, 2000.

[3] H. Chanson. *Hydraulics of Open Channel Flow*. Elsevier, May 2004.

[4] M. H. Chaudhry. *Open-Channel Flow*. Springer US, Boston, MA, 2008.

[5] F. Dubois, N. Petit, and P. Rouchon. Motion planning and nonlinear simulations for a tank containing a fluid. In *1999 European Control Conference (ECC)*, pages 3232–3237. IEEE, 1999.

[6] W. H. Graf and M. S. Altinakar. *Fluvial Hydraulics: Flow and Transport Processes in Channels of Simple Geometry*. Wiley, Oct. 1998.

[7] J. Kopp and F. Woittennek. Flatness based trajectory planning and open-loop control of shallow-water waves in a tube. *Automatica*, 122:109251, Dec. 2020.

[8] P. Kotyczka. Finite volume structure-preserving discretization of 1d distributed-parameter port-hamiltonian systems. *IFAC-PapersOnLine*, 49(8):298–303.

[9] A. Lew, J. E. Marsden, M. Ortiz, and M. West. Variational time integrators. *International Journal for Numerical Methods in Engineering*, 60(1):153–212, 2004.

[10] A. Maranzoni and M. Tomirotti. New formulation of the two-dimensional steep-slope shallow water equations. Part I: Theory and analysis. *Advances in Water Resources*, 166:104255, Aug. 2022.

[11] L. Mayer, J. Wurm, and F. Woittennek. Control-oriented models of the shallow water equationsusing energy-conserving discretization schemes. *PAMM*, 23(4):e202300267, 2023.

[12] R. Moulla, L. Lefévre, and B. Maschke. Pseudo-spectral methods for the spatial symplectic reduction of open systems of conservation laws. *Journal of Computational Physics*, 231(4):1272–1292, Feb. 2012.

[13] A. N. Nazarov. Mathematical modeling of a snow-powder avalanche in the framework of the equations of two-layer shallow water. *Fluid Dynamics*, 26(1):70–75, Jan. 1991.

[14] C. Pöll and I. Hafner. Index reduction and regularisation methods for multibody systems. 48(1):306–311.

[15] N. Petit and P. Rouchon. Dynamics and solutions to some control problems for water-tank systems. *IEEE Transactions on Automatic Control*, 47(4):594–609, Apr. 2002.

[16] A.-J.-C. B. d. Saint-Venant. *Théorie du mouvement non permanent des eaux, avec application aux crues des rivières et à l'introduction des marées dans leur lit*. Gauthier-Villars.

[17] J. Wurm, L. Mayer, and F. Woittennek. Feedback control of water waves in a tube with moving boundary. *European Journal of Control*, 62:151–157, 2021. Publisher: Elsevier Ltd.

[18] J. Wurm and F. Woittennek. Energy-based Modeling and Simulation of Shallow Water Waves in a Tube with Moving Boundary. *IFAC-PapersOnLine*, 55(20):91–96, Jan. 2022. Publisher: Elsevier.